Eurographics Symposium on Geometry Processing 2017
Fast Track submission to Computer Graphics Forum
K. Karciauskas, J. Peters

Volume 0 (1981), Number 0

A new class of guided C^2 subdivision surfaces combining good shape with nested refinement

Kęstutis Karčiauskas[a] and Jörg Peters[b]

[a] Vilnius University [b] University of Florida

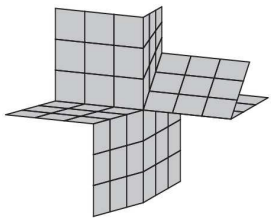

(a) control net (central valence $n = 7$)

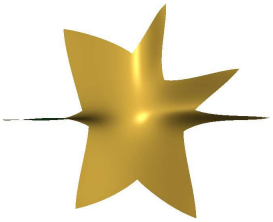

(b) G^1 guide surface

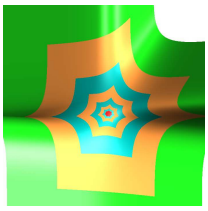

(c) C^2 subdivision rings

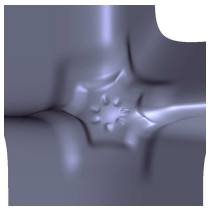

(d) embossed pattern based on refinement

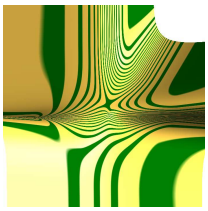

(e) Catmull-Clark: highlight line distribution and zoom

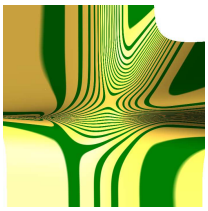

(f) Guided Subdivision: highlight line distribution and zoom

Figure 1: *Construction and comparison of guided subdivision: (a) input quad mesh (c-net) that is converted to (c) a regular (green) bi-3 region and an irregular subdivision region following a (b) guide surface. The guide surface does not match the bi-3 spline but defines the shape by joining polynomial pieces with curvature continuity (G^2); (c) shows six subdivision rings (alternating gold and cyan) completed by a finite polynomial (red) surface cap; (d) the embossed pattern exploits the degrees of freedom in the subdivision rings. (e) Catmull-Clark vs (f) guided subdivision: improving the highlight line distribution.*

Abstract

Converting quadrilateral meshes to smooth manifolds, guided subdivision offers a way to combine the good highlight line distribution of recent G-spline constructions with the refinability of subdivision surfaces. This avoids the complex refinement of G-spline constructions and the poor shape of standard subdivision. Guided subdivision can then be used both to generate the surface and hierarchically compute functions on the surface.

Specifically, we present a C^2 subdivision algorithm of polynomial degree bi-6 and a curvature bounded algorithm of degree bi-5. We prove that the common eigen-structure of this class of subdivision algorithms is determined by their guide and demonstrate that their eigenspectrum (speed of contraction) can be adjusted without harming the shape.

For practical implementation, a finite number of subdivision steps can be completed by a high-quality cap. Near irregular points this allows leveraging standard polynomial tools both for rendering of the surface and for approximately integrating functions on the surface.

Categories and Subject Descriptors (according to ACM CCS):

1. Introduction

The automatic conversion of quad meshes into C^2 surfaces of good shape and with built-in refinability addresses challenges of design and engineering analysis. Catmull-Clark subdivision offers refinability but the highlight line distributions of the resulting surfaces are often deficient, see Fig. 1e. Recent G-spline constructions, that use finitely many polynomial pieces, provide a good highlight line distribution but require a change of variables between the polynomial pieces and therefore careful book-keeping during refinement. A decade-old technique, guided subdivision [KP07], can in principle combine advances in shape with refinability by separating shape finding from the mathematical smoothness constraints of the final output surface: guided subdivision first decides on the shape by constructing a guide surface that need neither exactly fit to the surrounding surface nor necessarily be smooth everywhere; it then uses the flexibility of the sequence of subdivision rings (see Fig. 2) to smoothly connected to the surrounding surface and between rings while absorbing extra degrees of freedom by closely approximating the guide shape. The present algorithm improves on the shape and structure of the original guided subdivision constructions by addressing the main challenge of the approach: when deriving the sequence of contracting guided subdivision surface rings a careful reparameterization of the guide surface is required to collect the guide's derivatives since the guide and the rings have non-aligned parameter lines. The parameterization and sampling approach of this paper transfers the desirable highlight line distribution of an advanced G-spline construction [KP15] to the C^2 surface so that the new guided construction combines the natural refinement of subdivision with good shape. Just as for B-splines, the approach allows trading polynomial degree for smoothness and flexibility: if a user chooses the degree to be bi-6 then the guided subdivision surface is everywhere C^2; if the user choses the degree to be one of bi-5, bi-4 or bi-3 the surface has decreasing flexibility and is C^2 except for the central extraordinary point where it is C^1 and has bounded curvature.

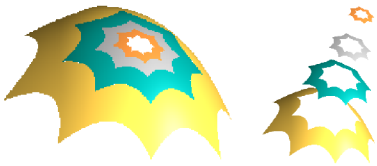

Figure 2: *(left) Subdivision surface (from [KP07]) built from (right) a sequence of contracting surface rings.*

Remarkably, the new guided subdivision constructions have a simple eigenstructure that is determined by the guide. In particular, the eigenspectrum and with it the speed of contraction can be adjusted without harming the shape. For example, the surface rings that make up the subdivision surface can be made to uniformly contract by 1/2 regardless of the valence. For practical use, a sequence of guided subdivision rings can be capped by a few polynomial pieces with good highlight line distribution. All localized refinement then takes place outside the (minuscule) cap where the rings form a regular C^2 surface. In summary, the new guided subdivision scheme

- is C^2 everywhere and at the extraordinary point curvature continuous for degree bi-6, or curvature bounded if the degree is chosen to be bi-5, bi-4, or bi-3;

and differs from earlier guided subdivision constructions in that it

- inherits an excellent highlight line distribution;
- has an explicit eigenstructure;
- the contraction speed of the subdivision rings (eigenspectrum) can be adjusted, e.g. uniformly $1/2$ regardless of valence;
- and a finite number subdivision rings can be combined with a small G-constructed cap to form a practical hybrid surface.

Overview. After a review of the closely-related literature, Section 2 introduces the notation and jet-sampling, an important tool used in the surface construction. Section 3 defines a G^2 surface $\mathbf{g}$ that has the correct structure to serve as a subdivision guide surface and closely approximates the G^1 surface of [KP15]; and it defines the algorithm for generating a sequence of nested guided subdivision rings. Section 3.3 sketches efficient implementation using pretabulation. Section 3.4 explains the hybrid construction. Section 4 tests the construction on an obstacle course and Section 5 provides the complete eigendecompostion of the guided subdivision algorithm. Section 6 discusses alternative choices considered and how functions on the surfaces can be refined.

1.1. Related Literature

Starting with [Doo78, CC78] (and [Loo87] for triangulations), subdivision surfaces have become dominant in the animation industry (see e.g. [DKT98, NLMD12]) and have inspired many polyhedral geometry processing algorithms and vice versa [WS04]. Shape control, e.g. via semi-smooth creases, have had a stronger impact than formal smoothness: except in pockets of academia, extensions of Catmull-Clark-subdivision to C^2 continuity [Lev06, Zor06, KP07] have largely been ignored.

Two new developments re-kindle the interest in higher-order smooth subdivision: isogeometric computations on surfaces and advances in quad meshing. Following the early lead of [COS00] more recently subdivision surfaces have been used as computational domains, see e.g. [Bar13, PXXZ16, RSAF16, JMPR16]. Quad meshing [BLP*12, VCD*16] has matured over the past decade starting with leveraging directional fields [MPZ14, PPM*16]. Such meshes provide natural input for guided subdivision surfaces. The use of guided subdivision surface s can be traced back to [Lev06], where the guide is a single polynomial and [KP07] where the guide is allowed to be any piecewise smooth function, piecewise polynomial in particular. The critical ingredients for good shape, measured via uniform curvature and highlight line distribution, are a well-shaped guide and its careful sampling.

2. Definitions and Setup

Analogous to Catmull-Clark-subdivision, we consider the input a network of quadrilateral facets or *quads*. Nodes where four quads meet are called regular, otherwise *irregular nodes*. Our focus is on the neighborhood of irregular nodes: a 2-ring of quads surrounding an irregular node that we call a *c-net*. The 1-ring of a c-net consists

of regular nodes and the c-net has $n \neq 4$ sectors. For example the interior nodes of Fig. 1a form a c-net.

The subdivision surface will be expressed piecewise in terms of tensor-product polynomials $\mathbf{p}$ of bi-degree d in Bernstein-Bézier (BB) form

$$\mathbf{p}(u,v) := \sum_{i=0}^{d}\sum_{j=0}^{d} \mathbf{p}_{ij} B_i^d(u) B_j^d(v), \quad (u,v) \in \square := [0..1]^2,$$

where $B_k^d(t) := \binom{d}{k}(1-t)^{d-k}t^k$ are the Bernstein-Bézier (BB) polynomials of degree d and $\mathbf{p}_{ij}$ are the BB coefficients [Far02, PBP02]. A central role will be played by the *corner jet constructor*

$$[f]^d_{j\times j}(u_0,v_0)$$

that expresses the expansion of a function f at (u_0,v_0) up to order $j-1$ in u and $j-1$ in v in BB-form of degree bi-d, i.e. by $j \times j$ BB-coefficients (see Fig. 3).

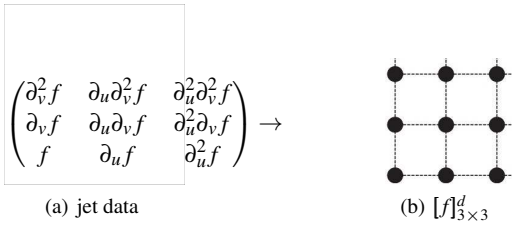

(a) jet data (b) $[f]^d_{3\times 3}$

Figure 3: *The partial derivatives in (a) are represented by BB-coefficients of the corner jet in (b).*

Fig. 4a displays four corner jet constructors $[f]^5_{3\times 3}$ merged to form a bi-5 patch and Fig. 4b displays four corner jet constructors $[f]^6_{4\times 4}$ merged to form a bi-6 patch by averaging the overlapping BB-coefficients.

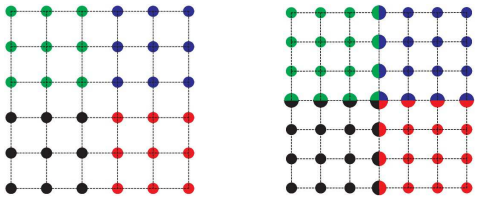

(a) bi-5 (b) bi-6

Figure 4: *(a) bi-5 patch assembled from 3×3 jets; (b) bi-6 patch assembled by averaging 4×4 jets.*

3. Construction of guided surfaces

The key to good shape is to construct and judiciously reparameterize a guide surface so that the jet constructors can form well-shaped subdivision rings, i.e. a sequence of surface annuli in $\mathbb{R}^3$ that join smoothly leaving an ever smaller central hole (see Fig. 2). Our final implementation combines pre-computed tables for the generating functions so that no system of equations needs to be solved and the response is immediate just like B-spline surfaces.

This section covers the more complex, but once and for all *derivation* of the construction. The derivation consists of two conceptual stages. Section 3.1 shows how to define a G^2 surface $\mathbf{g}$ that has the correct structure to serve as a subdivision guide surface and closely approximates the G^1 surface of [KP15]. (Constructing good guiding shapes is possible without reference to [KP15] but presentation takes considerably more space than the current one.) Section 3.2 shows how to repeatedly sample $\mathbf{g}$ to generate a sequence of nested subdivision rings with continuity properties summarized in Proposition. 1.

After Section 3.2 formally states the algorithm, Section 3.3 outlines how one can use pre-tabulation and the well-known de Casteljau algorithm to efficiently implement guided subdivision. Section 3.4 points out that in practice it may be useful to apply only a finite, user-chosen number of subdivision steps since the remaining minuscule hole can be capped by a G-construction of finitely many polynomial pieces. All localized refinement can then take place in the regular setting of the C^2 joined rings.

3.1. Guide surface

In this section, we create a G^2 guide surface $\mathbf{g}$ of degree bi-5 for filling a multi-sided hole by a series of rings sampled from $\mathbf{g}$.

Denote by L the linear shear that maps a unit square to the unit parallelogram with opening angle $\frac{2\pi}{n}$. Abbreviating $\mathsf{c} := \cos\frac{2\pi}{n}$ set $\grave{\mathbf{f}} := L$ and let $\acute{\mathbf{f}}$ be its reflection across the edge $v=0$, Fig. 5a. Then, along the common boundary $v=0$,

$$\partial_v \acute{\mathbf{f}} + \partial_v \grave{\mathbf{f}} - 2\mathsf{c}\partial_u \grave{\mathbf{f}} = 0, \tag{1}$$

$$\partial_v^2 \acute{\mathbf{f}} - \partial_v^2 \grave{\mathbf{f}} + 4\mathsf{c}\partial_u\partial_v \grave{\mathbf{f}} - 4\mathsf{c}^2\partial_u^2 \grave{\mathbf{f}} = 0. \tag{2}$$

The constraints (1) and (2) are 'unbiased' in the sense that exchanging $\acute{\mathbf{f}}$ and $\grave{\mathbf{f}}$ does not alter the equations. For degree bi-5 polynomials $\grave{\mathbf{f}}$ and $\acute{\mathbf{f}}$, the equations (1) and (2) yield a system of 12 linear equations in the BB-coefficients $\grave{\mathbf{p}}_{ij}$ and $\acute{\mathbf{p}}_{ij}$. These equations are solved symbolically, leaving as unconstrained the BB-coefficients marked in Fig. 5b by red or black bullets plus one circled cross.

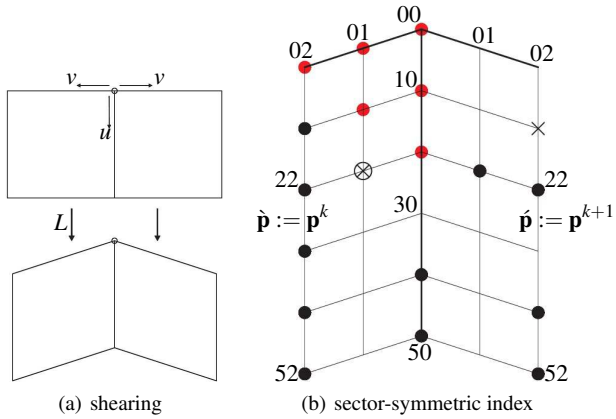

(a) shearing (b) sector-symmetric index

Figure 5: *(a) Linear shear L; (b) bi-5 solution to the local G^2 constraints: the unconstrained BB-coefficients are marked as red or black bullets or a circled cross.*

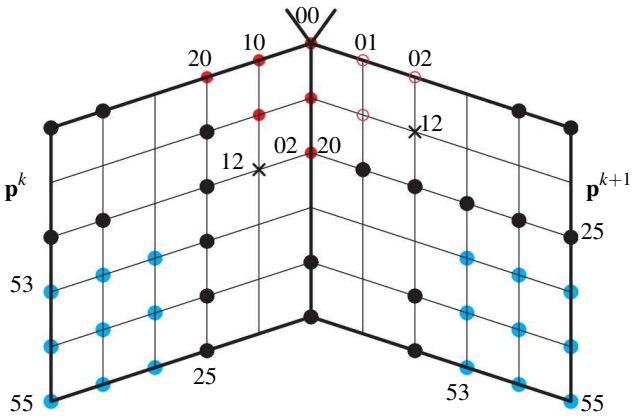

Figure 6: *Rotationally-symmetric indexing of the set $\mathcal{P}$ of the G^2 guide $\mathbf{g}$. BB-coefficients marked as cyan disks are unconstrained by local G^2 requirements.*

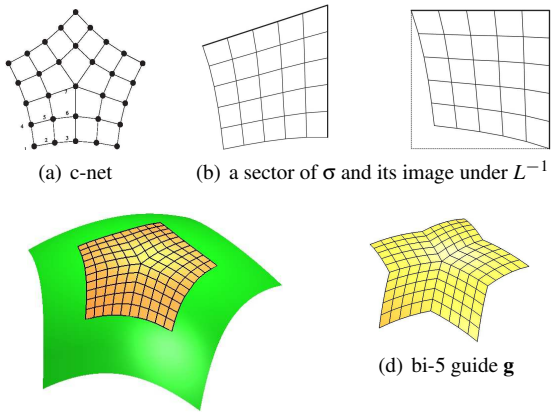

(a) c-net (b) a sector of σ and its image under L^{-1} (c) surrounding surface and $\mathbf{G}$ (d) bi-5 guide $\mathbf{g}$

Figure 7: *Construction of the guide surface. (c) the surrounding green bi-3 surface and in gold the bi-5 surface $\mathbf{G}$ of [KP15]. (d) The net of control points $\mathbf{g}^k_{ij}$ (not of final $\mathbf{b}^k_{ij}$).*

The interactions between the n local systems of equations at the irregular point $\grave{\mathbf{p}}_{00}$ are resolved by selecting six BB-coefficients $\mathbf{p}^k_{ij}$, $0 \le i+j \le 2$ for $k=0$ and so defining a quadratic expansion at the central extraordinary point; the BB-coefficients $\mathbf{p}^k_{ij}$, $0 \le i+j \le 2$, for $k>0$, are then defined recursively as

$$
\begin{aligned}
&\acute{\mathbf{p}}_{00} := \grave{\mathbf{p}}_{00}\,, \quad \acute{\mathbf{p}}_{10} := \grave{\mathbf{p}}_{10}\,, \quad \acute{\mathbf{p}}_{20} := \grave{\mathbf{p}}_{20}\,;\\
&\acute{\mathbf{p}}_{01} := -\grave{\mathbf{p}}_{01} + 2\mathsf{c}\grave{\mathbf{p}}_{10} + 2(1-\mathsf{c})\grave{\mathbf{p}}_{00}\,;\\
&\acute{\mathbf{p}}_{11} := -\grave{\mathbf{p}}_{11} + \frac{8\mathsf{c}}{5}\grave{\mathbf{p}}_{20} + (2-\frac{6\mathsf{c}}{5})\grave{\mathbf{p}}_{10} - \frac{2\mathsf{c}}{5}\grave{\mathbf{p}}_{00}\,; \qquad (3)\\
&\acute{\mathbf{p}}_{02} := \grave{\mathbf{p}}_{02} - 5\mathsf{c}\grave{\mathbf{p}}_{11} + 4\mathsf{c}^2\grave{\mathbf{p}}_{20} + (5\mathsf{c}-4)\grave{\mathbf{p}}_{01} + \mathsf{c}(9-8\mathsf{c})\grave{\mathbf{p}}_{10}\\
&\qquad + (4-9\mathsf{c}+4\mathsf{c}^2)\grave{\mathbf{p}}_{00}\,.
\end{aligned}
$$

Assigning, in each local system,

$$
\begin{aligned}
\acute{\mathbf{p}}_{12} := &\grave{\mathbf{p}}_{12} - 2\mathsf{c}\grave{\mathbf{p}}_{21} + 2\mathsf{c}\acute{\mathbf{p}}_{21} + \mathsf{c}\grave{\mathbf{p}}_{01} + (3\mathsf{c}-4)\grave{\mathbf{p}}_{11} + \frac{4}{5}\mathsf{c}(4-3\mathsf{c})\grave{\mathbf{p}}_{20}\\
&+ (4 - \frac{27}{5}\mathsf{c} + \frac{4}{5}\mathsf{c}^2)\grave{\mathbf{p}}_{10} + \frac{c}{5}(8\mathsf{c}-9)\grave{\mathbf{p}}_{00}, \qquad (4)
\end{aligned}
$$

yields a circulant system of n linear equations in $\mathbf{p}^k_{12}$ (since $\mathbf{p}^k_{12} = \grave{\mathbf{p}}_{21}$, $\mathbf{p}^{k+1}_{12} = \acute{\mathbf{p}}_{12}$; see rotationally-symmetric indexing in Fig. 6). This system has a unique solution (unless $n=3,6$ when one $\mathbf{p}^k_{12}$, say $\mathbf{p}^0_{12}$, is additionally free to choose). The explicit expressions for $\grave{\mathbf{p}}_{30}$, $\grave{\mathbf{p}}_{31}$, $\acute{\mathbf{p}}_{31}$, $\acute{\mathbf{p}}_{32}$, $\grave{\mathbf{p}}_{41}$, $\acute{\mathbf{p}}_{41}$, $\grave{\mathbf{p}}_{51}$, $\acute{\mathbf{p}}_{51}$ are presented in Appendix A.

Denote by $\mathcal{P}$ the set of BB-coefficients unconstrained by the G^2 constraints. We define $n^* := n+1$ whenever the valence $n \in \{3,6\}$ and $n^* = n$ otherwise. The elements of $\mathcal{P}$ are shown in Fig. 6: six red bullets for the quadratic expansion, $8n+n^*$ black bullets, and, in each sector corner, 3×3 cyan bullets that do not affect G^2 continuity between sectors. The elements of $\mathcal{P}$ are pinned down to best approximate the bi-5 surface $\mathbf{G}$ of the c-net as defined in [KP15]. Let $\sigma : \mathbb{R}^{2\times n} \to \mathbb{R}^2$ be the $2\pi/n$-rotationally symmetric map obtained by applying the algorithm of [KP15] to the control points of the planar characteristic c-net of Catmull-Clark-subdivision shown in Fig. 7a. Fig. 7b, *left*, shows one sector of σ for $n=5$ and Fig. 7b, *right* shows $L^{-1}\circ\sigma$ to be used for sampling the guide $\mathbf{g}$.

Setting the central point of $\mathbf{g}$ to the central point of $\mathbf{G}$, we collect the $5+8n+n^*+9n$=$17n+n^*+5$ unconstrained BB-coefficients of the set $\mathcal{P}$. Sampling the kth sector according to $[\mathbf{g}^k \circ L^{-1} \circ \sigma]^5_{3\times 3}$ at all four corners of each unit square sub-domain of σ, we obtain the BB-coefficients $\mathbf{b}^k_{ij}$, $k=0,\ldots,n-1$, $i,j=0,\ldots,5$. The $\mathbf{b}^k_{ij}$ are linear expressions in $\mathcal{P}$ and we assemble them to form n patches $\mathbf{b}^k$ of degree bi-5. Then $\mathcal{P}$ is the least-squares solution of minimizing the sum of differences between each $\mathbf{b}^k_{ij}$ and its corresponding coefficient of $\mathbf{G}$. This defines the G^2 guide surface for C^2 subdivision (of the chosen degrees bi-6, bi-5, bi-4 or bi-3).

3.2. Parameterization and guided surface rings

The guide $\mathbf{g}$ was constructed to facilitate filling the multi-sided hole by a contracting sequence of sampled guided rings. The construction, see Fig. 8, leverages the fact that the characteristic ring χ of Catmull-Clark subdivision joins C^2 to its scaled copy $\lambda\,\chi$, where $\lambda := \frac{1}{16}\left(\mathsf{c}+5+\sqrt{(\mathsf{c}+1)(\mathsf{c}+9)}\right)$ is the subdominant eigenvalue of Catmull-Clark subdivision. Since the shear L is linear, also $L^{-1}\circ\chi$ is C^2-connected to its scaled copy $\lambda(L^{-1}\circ\chi)$ (see Fig. 8d). Moreover, the outer second-order Hermite data of $L^{-1}\circ\chi$ (underlaid gray in Fig. 8a) is determined by the C^2 prolongation $L^{-1}\circ(\lambda^{-1}\chi)$ and binary splitting (see Fig. 8c).

Subdivision Algorithm.
Input: a sector $\mathbf{g}^k$ of guide $\mathbf{g}$.
Output: BB-coefficients of three bi-d ($d=5$ or $d=6$) patches in the k-th sector of the lth subdivision ring $\mathbf{x}^l$, $l=0,\ldots$.
Bi-5 Algorithm: sample $[\mathbf{g}^k \circ (L^{-1}\circ\lambda^l\chi)]^5_{3\times 3}$ at the inner corners marked by bullets in Fig. 8a to obtain the bi-5 coefficients of Fig. 8c underlaid white; sample $[\mathbf{g}^k \circ (\lambda^l\tilde{\chi})]^5_{3\times 3}$ at the outer corners marked by circles in Fig. 8b and mid-split the resulting bi-5 data to obtain the bi-5 coefficients of Fig. 8c underlaid gray. The first of these gray sets of BB-coefficients ($l=0$) is replaced by C^2 prolongation from the surrounding surface.

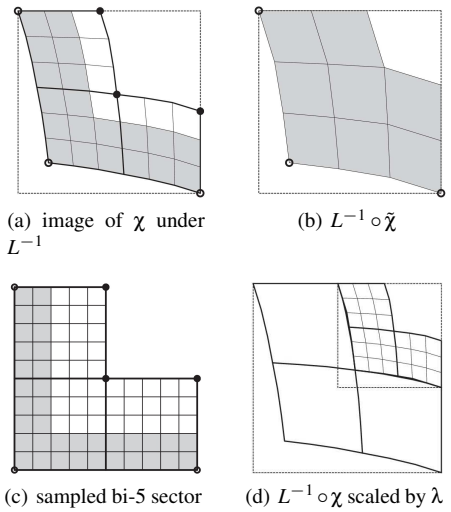

(a) image of χ under L^{-1} (b) $L^{-1}\circ\tilde{\chi}$ (c) sampled bi-5 sector (d) $L^{-1}\circ\chi$ scaled by λ

Figure 8: ***Construction of guided ring.***

The bi-6 algorithm is identical, except that $[\mathbf{g}^k\circ(L^{-1}\circ\lambda^l\chi)]^6_{4\times4}$ is sampled and assembled according to Fig. 4b.

In summary, guided subdivision has the following continuity properties.

Proposition 1 The Subdivision Algorithm fills a multi-sided hole in a spline surface C^2 up to the central extraordinary point. If the degree is bi-6, the surface is C^2; if the degree is bi-5, the surface is C^2 except for the central point where it is C^1 and curvature bounded.

Proof Since χ is C^2 and since the G^1 and G^2 constraints (1) and (2) that tie together pieces of L tie together adjacent sectors of $\mathbf{g}$, adjacent sectors join C^2. Due to prolongation, consecutive rings are C^2-connected and so is the first ring to the surrounding spline surface. The limit point characterization follows by the arguments of [KP07, Thm 1] applied to $(\mathbf{g}\circ L^{-1})\circ\chi$. □

The good shape of $\mathbf{G}$ constructed according to [KP15] is retained since the guide $\mathbf{g}$ closely approximates the surface $\mathbf{G}$.

3.3. Efficient Implementation

An efficient implementation focuses on the generating functions $\mathbf{g}^k$ of the guided subdivision surface defined as follows. It suffices to look at one coordinate. Assign to all $\mathbf{c}$-net nodes the value 0 except for $\mathbf{c}^0_m=1$ for one of $m=1,\ldots,7$ (see Fig. 7(a) for the labeling). Apply the algorithm to compute for each m the scalars

$$h^{k,m}_{ij}\in\mathbb{R},\ k=0,\ldots,n-1,\ m=1,\ldots,7,\ i,j\in\{0,\ldots,5\},$$

where $h^{0,7}_{ij}=\ldots=h^{n-1,7}_{ij}$. Then BB-coefficients of the surface are

$$\mathbf{g}^s_{ij}:=h^{0,7}_{ij}\mathbf{c}^0_7+\sum_{k=0}^{n-1}\sum_{m=1}^{6}h^{k,m}_{ij}\mathbf{c}^{s-k}_m,$$

where the superscript of $\mathbf{c}^{s-k}_m$ is interpreted modulo n.

Computing $[\mathbf{g}^k\circ(L^{-1}\circ\lambda\chi)]^5_{3\times3}$ for the bi-5 Subdivision Algorithm is equivalent to (i) linearly mapping $S:[0..1]^2\to[0..\lambda]^2$ and (ii) sampling $[(\mathbf{g}^k\circ S)\circ(L^{-1}\circ\chi)]^5_{3\times3}$ and $[(\mathbf{g}^k\circ S)\circ(L^{-1}\circ\tilde{\chi})]^5_{3\times3}$. In Step (i) applying de Casteljau's algorithm at $u=\lambda=v$ yields the BB-coefficients of $\mathbf{g}^k\circ S$ as an affine combination of $\mathbf{g}^k$. This affine $6^2\times6^2$ map is tabulated.
For (ii), for each valence n, a generic sector of the guided subdivision ring is pre-computed. This sector consists of three patches of degree bi-5 and is stored as a table of size $3(6^2\times\cdot6^2)$, by sampling $[\mathbf{g}^k\circ(L^{-1}\circ\chi)]^5_{3\times3}$ and $[\mathbf{g}^k\circ(L^{-1}\circ\tilde{\chi})]^5_{3\times3}$ in terms of symbolic $\mathbf{g}^k_{ij}$. Analogously, for bi-6 subdivision, we pre-compute for each valence n a table of size $3(7^2\times7^2)$.

If the storage of the pre-computed data is a concern, the majority of the entries can be derived by C^2 prolongation from the previous ring. The remainder is defined by two jets in each sector, one of which has diagonal symmetry. For bi-5 subdivision, performing these simple extra steps reduces the tabulation for each valence by a factor of ~7 from $3(6^2\times6^2)$ to $15*6^2$. Computing $[\mathbf{g}^k\circ(L^{-1}\circ\lambda\chi)]^6_{4\times4}$ analogously yields an efficient implementation for the bi-6 variant.

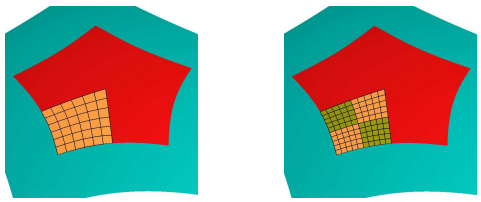

(a) bi-6 (b) bi-5

Figure 9: *G^1 caps for $n=5$. The cap is surrounded by the last ring produced by guided subdivision (light blue background).*

3.4. A Practical Hybrid

Being able to cap the subdivision surface after a few steps is useful in practice, already for visualization (see the next section). For Catmull-Clark subdivision the first refinement steps introduce highlight line distortions that no cap can repair. By contrast, guided subdivision retains good shape and enables capping without loss of shape quality. Fig. 9 shows the natural structure of these bi-6 and bi-5 caps (bi-5 caps with one patch per sector lead to reduced quality, hence the split). A prototypical construction, of a bi-6 cap, is detailed in Appendix B. The good shape of this finite hybrid representation makes them aesthetically useful in their own right and the finite number of polynomial surface pieces simplifies their use for downstream applications and to serve as a domain for surface-based computations.

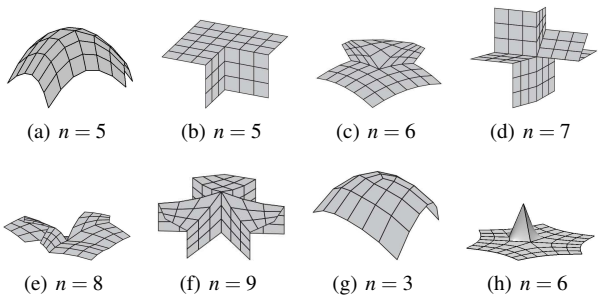

(a) $n = 5$ (b) $n = 5$ (c) $n = 6$ (d) $n = 7$

(e) $n = 8$ (f) $n = 9$ (g) $n = 3$ (h) $n = 6$

Figure 10: *Some challenging* **c***-nets.*

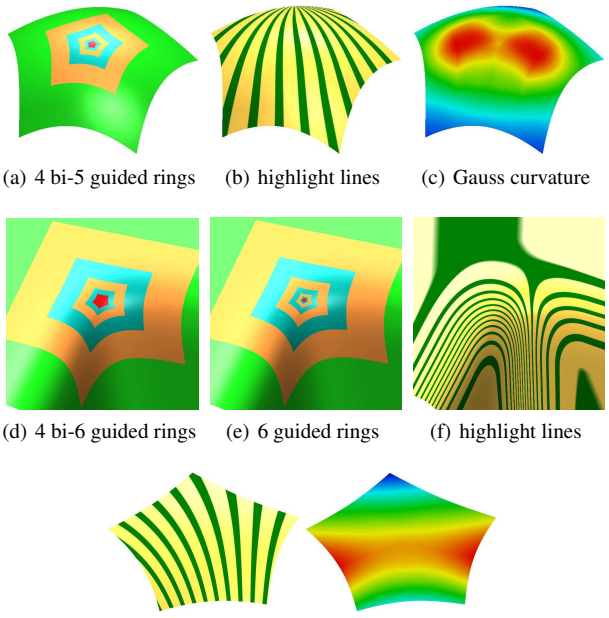

(a) 4 bi-5 guided rings (b) highlight lines (c) Gauss curvature

(d) 4 bi-6 guided rings (e) 6 guided rings (f) highlight lines

(g) zoom of (d): highlights and mean curvature

Figure 11: *Guided rings and central cap (in red) for $n = 5$:* top *row: c-net of Fig. 10a* middle, bottom *rows: c-net of Fig. 10b.*

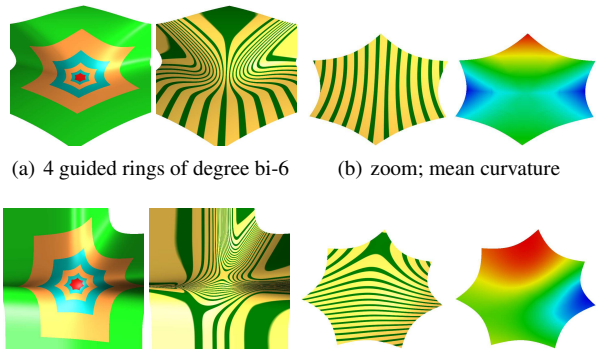

(a) 4 guided rings of degree bi-6 (b) zoom; mean curvature

(c) 4 guided rings of degree bi-5 (d) zoom; Gauss curvature

Figure 12: *Guided subdivision rings, highlight lines and curvature; top row: bi-6 surfaces, $n = 6$, c-net Fig. 10c; bottom row: bi-5 surfaces, $n = 7$, c-net Fig. 10d.*

4. Examples

The Subdivision Algorithm is applied to the challenging c-nets presented in Fig. 10. Displaying the surrounding spline surface in green in Fig. 11 for valence $n = 5$, Fig. 12 for valences $n = 6, 7$, and Fig. 13 for valences $n = 8, 9$ and $n = 3$, demonstrates that we do not just create good caps for the various n, but caps that transition well from the input data. The finite caps of the hybrid representation are red. 'Zoom' indicates that innermost guided ring and the finite cap are displayed. The zoom demonstrates that even the caps have a calm curvature distribution, quite in contrast to Catmull-Clark-subdivision, where the shape deficiencies are acerbated at each step. Fig. 14 juxtaposes the G^1 surface [KP15] that defines the shape via the guide **g** and the corresponding guided subdivision surface. This illustrates the fact that the highlight line distribution of [KP15] and the subdivision surface are visually almost identical, even on very challenging input nets.

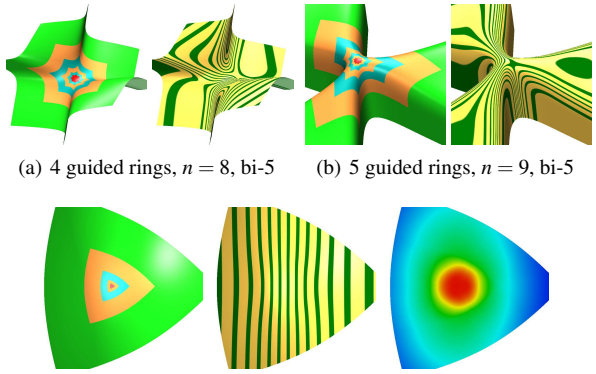

(a) 4 guided rings, $n = 8$, bi-5 (b) 5 guided rings, $n = 9$, bi-5

(c) 3 guided rings, $n = 3$, bi-5, Gauss curvature

Figure 13: *Bi-5 guided subdivision surfaces for (a) $n = 8$, c-net Fig. 10e; (b) $n = 9$, c-net Fig. 10f; (c) $n = 3$, c-net Fig. 10g.*

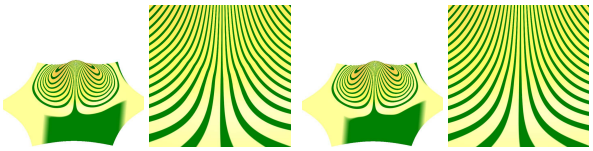

(a) [KP15] surface and zoom (b) 4 guided rings, bi-5

Figure 14: *Surfaces corresponding to c-net Fig. 10h: (a) [KP15] vs (b) this algorithm, bi-5 with 4 guided rings, zoom to the innermost two rings.*

5. Eigen-decomposition

The eigen-decomposition of guided subdivision differs from that of conventional subdivision such as Catmull-Clark, in that it is defined by the guide surface: any guided subdivision inherits the guide's eigen-decomposition. Therefore the decomposition does not overtly involve the specification of large circulant matrices or of characteristic polynomials; and the same analysis applies to

guided subdivision constructions of different polynomial degree. If we consider just one bi-5 patch of $\mathbf{g}$ without neighbor-interaction, the scaling by λ to the next-level subdivision ring (Section 3.2) yields, due to the monomial structure, eigenvalues λ^s for total degree $s = 0,\dots,10$ and eigenfunctions $u^i v^j$ of tensor-degree (i,j), $0 \le i,j \le 5$ (see Fig. 15). The eigen-analysis of a full ring is more complex due to the interaction between neighbors, but retains this basic structure.

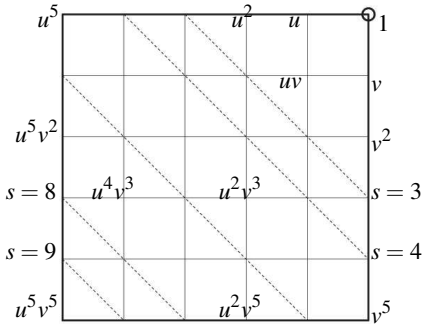

Figure 15: *Monomial structure of the local eigen-decomposition.*

The Subdivision Algorithm constructs the ℓth surface ring from a vector of BB-coefficients P_ℓ corresponding to the set $\mathcal{P}$ of the guide $\mathbf{g}$ restricted to $[0..\lambda^\ell]^2$. With M the map so that $P_\ell = MP_{\ell-1}$, the eigen-decomposition determines w and μ so that $Mw = \mu w$. Appendix C shows that all eigenvalues μ are of the form λ^s where $0 < \lambda < 1$ is free to choose:

$\lambda^s, s=$	0	1	2	3	4	5,6,7,8	9	10
multiplicity	1	2	3	n^*	$2n$	$3n$	$2n$	n

(5)

where $n^* = n+1$ when $n \in \{3,6\}$ and $n^* = n$ otherwise. The

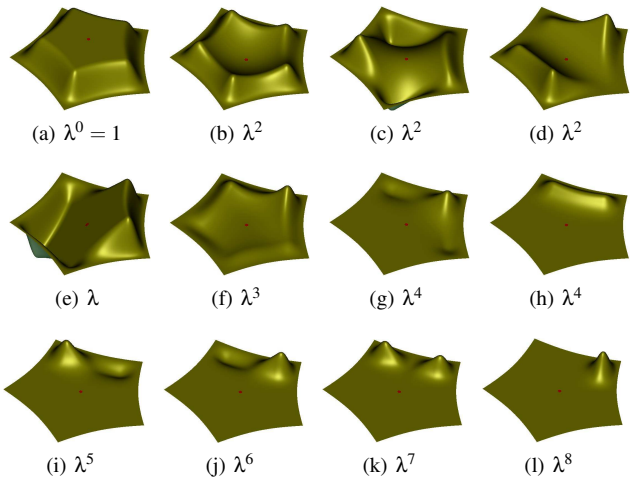

Figure 16: *Some bi-5 eigenfunctions for $n = 5$.*

bi-5 eigenfunctions for $n = 5$ shown in Fig. 16 are determined by setting one free parameter x_k^s (see Fig. 26) to 1 and all others to 0, completing this determining set to a smooth eigenring according to the Subdivision Algorithm, and generating six scaled copies before filling the center with a (red) cap. For λ^2 the functions in Fig. 16 are scaled in height and, at each level, we formed, linear combinations of the eigenrings to show the typical cup and two saddle shapes of the quadratic terms. After assembling the surface, the outermost BB-coefficients were set to zero.

Due to the index-rotational symmetry, for $s = 3,\dots 10$ only 23 $(= 17+1+5)$ eigenfunctions (besides the constant one for the eigenvalue 1) need to be tabulated. An exception to this symmetry is $s = 3$ when $n = 3,6$ and $26,29$ functions are required. Since the eigen-ring ℓ is obtained by multiplying the initial eigen-ring by $(\lambda^s)^\ell$, it suffices to store the initial eigen-ring. The ℓth surface ring is a linear combination of these $(\lambda^s)^\ell$-scaled eigen-rings.

6. Discussion

Here we discuss alternatives and options that were not given prominence in the main construction. We discuss reducing the degree of the guide (to simplify the eigenstructure), reducing the degree of the overall guided subdivision scheme, changing the speed of the contraction of the subdivision rings and refining functions on a guided subdivision surface.

6.1. Guides of lower degree

The degree of the subdivision surfaces is not strongly coupled to the degree of the guide surface. We can choose guides of degree bi-4 or bi-3 where the enforcement of (1) and (2) and the eigendecomposition are analogous to bi-5 case. Corresponding to the unconstrained control points for the guides $\mathbf{g}$ (cf. Fig. 17), we count

degree of $\mathbf{g}$	eigenfunctions
bi-5	$17n+6+n^*$
bi-4	$9n+6+n^*$
bi-3	$3n+6+n^*$

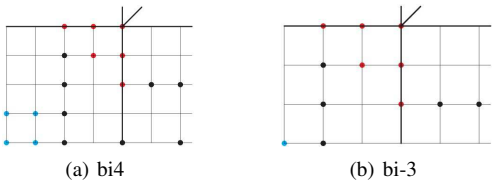

Figure 17: *The control points of G^2 guides of degree bi-4 and bi-3. Unconstrained points are marked as red and black disks.*

On one hand, lower degree simplifies the analysis while on the other hand, lower degree of an n-patch guide harms the surface quality as illustrated in Fig. 18 (no caps are added since the poorer highlight line distribution shows clearly in the subdivision rings). Fig. 18a shows that even an optimized bi-3 guide yields oscillating and sharp highlight lines.

We tested two approaches to improving the shape. Applying one step of bi-5 subdivision followed by a bi-3 guide improves results, see Fig. 18b; and twice repeating the bi-5 subdivision improves the highlight line distribution to Fig. 18c. The c-net of Fig. 10h, a single off-center spike, is notorious for revealing shortcomings of

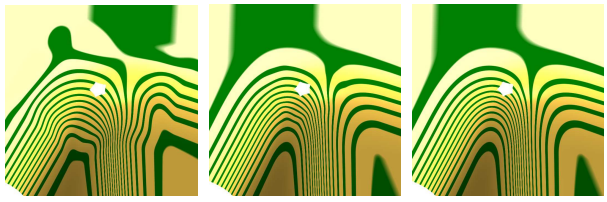

(a) 4 rings (guide bi-3) (b) (bi-5) + 3 (bi-3) (c) 2 (bi-5) + 2 (bi-3)

(d) rings (e) 4 (bi-5) (f) 4 (bi-4) (g) 2(bi-5) + 2 (bi-3)

Figure 18: *Comparison of bi-5 surfaces with 4 guided rings sampled from guides of different degrees. The central gap is not filled with a cap. The highlight line distribution of guided subdivision surfaces from top row: net Fig. 10b, bottom row: net Fig. 10h (5× pdf zoom recommended).*

surface constructions. Yet, the results (see Fig. 18 bottom row) of applying a bi-4 guide (after zero or one step of bi-5 subdivision) are difficult to distinguish from those of the bi-5 guide. By contrast, (full enlargement of) Fig. 18g shows oscillations of the highlight lines for a bi-3 guide even after two bi-5 preprocessing steps.

6.2. Bi-4 and bi-3 guided subdivision surfaces

For some applications, degree bi-5 may be considered a drawback. Leveraging the weak link between shape and smoothness, we introduce 2×2 macro patches for degree bi-4 and 3×3 macro patches for degree bi-3 (see Fig. 19) to enforce the C^2 prolongation between rings. The resulting surfaces are curvature bounded at the central point and preserve the highlight line distribution of the bi-5 construction well – at the cost of increasing the number of polynomial pieces by a factor of 4, respectively 9.

Notably, for the corresponding hybrid construction, the G^1 bi-3 caps are formally only C^0-connected to the last guided ring. Yet, the resulting highlight line distribution is without flaw (rightmost zoomed image of Fig. 20b); by contrast, enforcing exact C^1-continuity reduces the uniformity of the highlight line distribution.

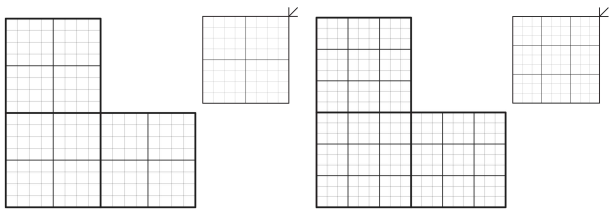

(a) bi-4 ring and cap (b) bi-3 ring and cap

Figure 19: *Macro-patches: one sector of the last guided subdivision ring and a cap, consisting of 2×2 respectively 3×3 pieces.*

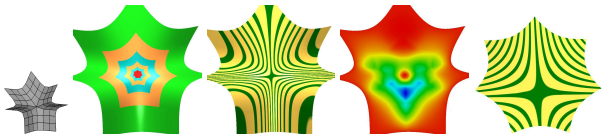

(a) bi-3: c-net, 4 guided rings, highlight lines and Gauss curvature

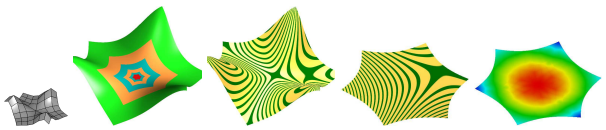

(b) bi-4: c-net, 4 guided rings, highlight lines and Gauss curvature

Figure 20: *Macro-patch constructions with (red) cap. Rightmost figures are zoomed in to the last ring plus cap.*

6.3. Changing the contraction speed

Using the subdominant eigenvalue λ of Catmull-Clark subdivision for σ implies that the contraction of guided rings becomes slower when the valence increases (Fig. 13b vs c). Using instead the characteristic map of [KP09], the eigenvalue can be set to $\frac{1}{2}$ for all valencies $n>4$ to yield a uniform contraction speed. Fig. 21 *top* vs *bottom* contrasts the characteristic map for Catmull-Clark subdivision and λ, with the uniform contraction by $\frac{1}{2}$ of [KP09]. Fig. 22a shows the same surface as Fig. 13a while Fig. 22b is constructed with contraction speed $1/2$. The latter has visually identical highlight lines, an observation that holds for all c-nets that we tested, including all of Fig. 10 (The increased contraction is evident from the size of the red caps.) Fig. 13b compares to Fig. 22d. All c-nets of Fig. 10 have a more uniform curvature distribution in the vicinity of the caps when using speed $1/2$.

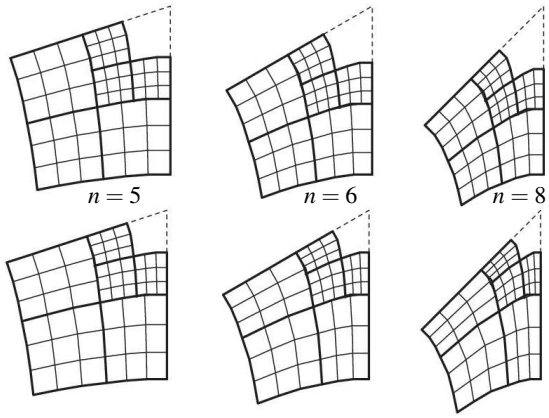

Figure 21: *Characteristic maps. top: Catmull-Clark-subdivision [CC78]; bottom: adjustable speed subdivision [KP09] with $\lambda := \frac{1}{2}$.*

6.4. Refinement for functions on guided subdivisions surfaces

With the shape of the subdivision surface determined by the c-net via $\mathcal{P}$ of the guide, here we define a nested space of refinable functions on the surface. The combinatorial layout of the functions is

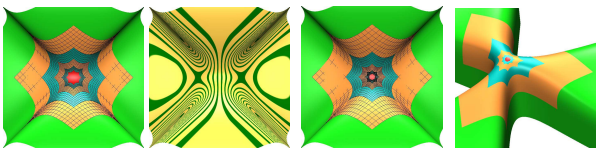

(a) [CC78] (b) [KP09]

Figure 22: *Four guided rings are generated before adding the red cap. The guided subdivision surface in (a) leverages the characteristic map of [CC78] while (c) uses the more uniform contraction of the characteristic map of [KP09]. (a,b left) net from Fig. 10e, (b right) net from Fig. 10f.*

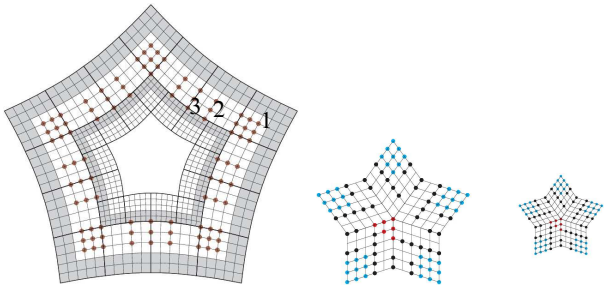

(a) d.o.f. of bi-5 C^2 ring (b) $\mathcal{P}$ and $\mathcal{P}$ of refined

Figure 23: *Structure of refinable functions on guided subdivision surfaces. (a) Degrees of freedom (brown bullets) in the C^2 bi-5 ring not influenced by the refined $\mathcal{P}$. The BB-coefficients in the gray layers are defined by C^2 expansion from the surrounding surface. (b) A guide set $\mathcal{P}$ exists at each refinement step.*

identical to that of the surfaces. For example, each refinement of the bi-5 construction yields $18n$ new degrees of freedom. In Fig. 23a, the BB-coefficients determined by C^2 extension inwards are underlaid in gray and the $18n$ free coefficients of the outermost subdivision ring that is no longer influenced by a once-refined set $\mathcal{P}$ are shown as brown bullets. Functions corresponding to the markers 1,2,3 are displayed in Fig. 24,b,c,d. (Standard bi-5 respectively bi-6 spline subdivision with triple knots can be applied to these rings in subsequent refinements.) In addition to the $18n$ new degrees of freedom, each subdivision step offers N degrees of freedom corresponding to the set $\mathcal{P}$. If the identity function is to be represented, the refined set $\mathcal{P}$ is obtained from its coarser predecessor Fig. 23b via de Casteljau's algorithm.

While eigendecomposition can be used to obtain finite expressions for computations on subdivision surfaces, the considerable number of terms make us think that most numerical computations are better served by computing with the hybrid representation after a suitable number of refinement steps.

7. Conclusion

The new guided subdivision surfaces offer an automatic conversion of quad meshes with irregular vertices into C^2 surfaces of good shape and built-in refinability. The construction of guided subdivision surfaces is conceptually simple, and has been implemented

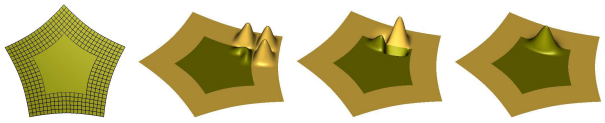

(a) filling (b) f_1 (c) f_2 (d) f_3

Figure 24: *(a) BB-coefficients of the innermost ring from Fig. 23a and the filling by subdivision. (b), (c), (d) Bi-5 functions f_j with the meaning of the subscripts indicated in Fig. 23a.*

and tested on challenging examples. The shape resulting from the tabulated refinement formulas of guided subdivision is generally better than that of small-stencil standard subdivision algorithms. Due to the guide shape, curvature distribution of the C^2 bi-6 and the near-C^2 bi-5 construction are typically indistinguishable. Alternatively, a hybrid surface consisting of finitely many polynomial pieces preserves the shape but is more readily amenable to subsequent computations on the surface. The eigen-structure of this class of subdivision algorithms is determined by the guide and fully analyzed. The speed of contraction can be adjusted without harming the shape.

Acknowledgements This work was supported in part by DARPA grant HR00111720031.

References

[Bar13] BARENDRECHT P. J.: *IsoGeometric Analysis with Subdivision Surfaces*. PhD thesis, MS Thesis, Technical University of Eindhoven, 2013. 2

[BLP*12] BOMMES D., LÉVY B., PIETRONI N., PUPPO E., SILVA C., TARINI M., ZORIN D.: State of the art in quad meshing. In *Eurographics STARS* (2012). 2

[CC78] CATMULL E., CLARK J.: Recursively generated B-spline surfaces on arbitrary topological meshes. *Computer Aided Design 10* (1978), 350–355. 2, 8, 9

[COS00] CIRAK F., ORTIZ M., SCHRÖDER P.: Subdivision surfaces: A new paradigm for thin-shell finite-element analysis. *Internat. J. Numer. Methods Engrg. 47*, 12 (2000), 2039–2072. 2

[DKT98] DEROSE T., KASS M., TRUONG T.: Subdivision surfaces in character animation. In *SIGGRAPH '98: Proceedings of the 25th annual conference on Computer graphics and interactive techniques* (New York, NY, USA, 1998), ACM Press, pp. 85–94. 2

[Doo78] DOO D.: A subdivision algorithm for smoothing down irregularly shaped polyhedrons. In *Int'l Conf. Ineractive Techniques in Computer Aided Design* (Bologna, Italy, 1978), IEEE Computer Soc., pp. 157–165. 2

[Far02] FARIN G.: *Curves and Surfaces for Computer Aided Geometric Design: A Practical Guide*. Academic Press, San Diego, 2002. 3

[JMPR16] JÜTTLER B., MANTZAFLARIS A., PERL R., RUMPF M.: On numerical integration in isogeometric subdivision methods for PDEs on surfaces. *Computer Methods in Applied Mechanics and Engineering 302* (2016), 131–146. 2

[KP07] KARČIAUSKAS K., PETERS J.: Concentric tesselation maps and curvature continuous guided surfaces. *Computer Aided Geometric Design 24*, 2 (Feb 2007), 99–111. 2, 5

[KP09] KARČIAUSKAS K., PETERS J.: Adjustable speed surface subdivision. *Computer Aided Geometric Design. 26* (2009), 962–969. 8, 9

[KP15] KARČIAUSKAS K., PETERS J.: Improved shape for multi-surface blends. *Graphical Models 8* (2 2015), 87–98. 2, 3, 4, 5, 6

[Lev06] LEVIN A.: Modified subdivision surfaces with continuous curvature. *ACM Trans. Graph 25*, 3 (2006), 1035–1040. 2

[Loo87] LOOP C.: *Smooth subdivision surfaces based on triangles.* Master's thesis, Department of Mathematics, University of Utah, 1987. 2

[MPZ14] MYLES A., PIETRONI N., ZORIN D.: Robust field-aligned global parametrization. *ACM Trans. Graph. 33*, 4 (July 2014), 135:1–135:14. 2

[NLMD12] NIESSNER M., LOOP C. T., MEYER M., DEROSE T.: Feature-adaptive GPU rendering of catmull-clark subdivision surfaces. *ACM Trans. Graph 31*, 1 (2012). 2

[PBP02] PRAUTZSCH H., BOEHM W., PALUSZNY M.: *Bézier and B-spline techniques*. Springer Verlag, 2002. 3

[PPM*16] PIETRONI N., PUPPO E., MARCIAS G., SCOPIGNO R., CIGNONI P.: Tracing field-coherent quad layouts. *Computer Graphics Forum (special Issue of Pacific Graphics)* (2016). 2

[PXXZ16] PAN Q., XU G., XU G., ZHANG Y.: Isogeometric analysis based on extended Catmull-Clark subdivision. *Computers & Mathematics with Applications 71*, 1 (2016). 2

[RSAF16] RIFFNALLER-SCHIEFER A., AUGSDÖRFER U. H., FELLNER D. W.: Isogeometric shell analysis with NURBS compatible subdivision surfaces. *Applied Mathematics and Computation 272* (2016). 2

[VCD*16] VAXMAN A., CAMPEN M., DIAMANTI O., PANOZZO D., BOMMES D., HILDEBRANDT K., BEN-CHEN M.: Directional field synthesis, design, and processing. *Computer Graphics Forum* (2016). 2

[WS04] WARREN J. D., SCHAEFER S.: A factored approach to subdivision surfaces. *IEEE Computer Graphics and Applications 24*, 3 (2004), 74–81. 2

[Zor06] ZORIN D.: Constructing curvature-continuous surfaces by blending. In *Eurographics Symposium on Geometry Processing* (2006), Sheffer A., Polthier K., (Eds.), Eurographics Association, pp. 31–40. 2

A. Appendix

Let

$$d_1 := 4+8\mathsf{c}+5\mathsf{c}^2,\ d_2 := 4+5\mathsf{c},\ d_3 := 36+45\mathsf{c}+5\mathsf{c}^2,$$
$$d_4 := 20+36\mathsf{c}+9\mathsf{c}^2-15\mathsf{c}^3,\ d_5 := 32+48\mathsf{c}+15\mathsf{c}^2,$$
$$d_6 := 16+36\mathsf{c}+36\mathsf{c}^2+15\mathsf{c}^3,\ d_7 := 32+64\mathsf{c}+72\mathsf{c}^2+48\mathsf{c}^3+15\mathsf{c}^4.$$

Then

$$\grave{\mathbf{p}}_{30} := \frac{2}{3}\grave{\mathbf{p}}_{10}+\frac{c-5}{3\mathsf{c}}\grave{\mathbf{p}}_{20}+\frac{5}{6\mathsf{c}}\left(\grave{\mathbf{p}}_{21}+\acute{\mathbf{p}}_{21}\right);$$

$$\acute{\mathbf{p}}_{32} := \grave{\mathbf{p}}_{32}-\frac{d_6}{3d_1}\left(\grave{\mathbf{p}}_{11}-\acute{\mathbf{p}}_{11}\right)+\frac{d_7}{3\mathsf{c}d_1}\left(\grave{\mathbf{p}}_{21}-\acute{\mathbf{p}}_{21}\right)-\frac{d_6}{3\mathsf{c}d_1}\left(\grave{\mathbf{p}}_{22}-\acute{\mathbf{p}}_{22}\right)$$
$$-\frac{\mathsf{c}d_2}{2d_1}\left(\grave{\mathbf{p}}_{42}-\acute{\mathbf{p}}_{42}\right)+\frac{\mathsf{c}^2}{2d_1}\left(\grave{\mathbf{p}}_{52}-\acute{\mathbf{p}}_{52}\right);$$

$$\grave{\mathbf{p}}_{31} := \frac{2\mathsf{c}}{15}\grave{\mathbf{p}}_{00}+\frac{8\mathsf{c}}{15}\grave{\mathbf{p}}_{10}+\frac{2}{3}\grave{\mathbf{p}}_{11}-\frac{25+16\mathsf{c}^2}{15\mathsf{c}}\grave{\mathbf{p}}_{20}$$
$$+\frac{1+2\mathsf{c}}{6\mathsf{c}}\grave{\mathbf{p}}_{21}+\frac{3}{2\mathsf{c}}\acute{\mathbf{p}}_{21}+\frac{1}{3\mathsf{c}}\left(\grave{\mathbf{p}}_{22}-\acute{\mathbf{p}}_{22}\right)+\frac{2\mathsf{c}}{5}\grave{\mathbf{p}}_{40};$$

$$\grave{\mathbf{p}}_{41} := \frac{2\mathsf{c}}{15d_1}\left(\mathsf{c}d_2\grave{\mathbf{p}}_{00}-d_3\grave{\mathbf{p}}_{10}+5d_2\grave{\mathbf{p}}_{11}\right)$$
$$+\frac{4d_4}{15d_1}\grave{\mathbf{p}}_{20}-\frac{d_5}{6d_1}\grave{\mathbf{p}}_{21}-\frac{\mathsf{c}(16+25\mathsf{c})}{6d_1}\acute{\mathbf{p}}_{21}+\frac{d_2}{3d_1}\left(\grave{\mathbf{p}}_{22}-\acute{\mathbf{p}}_{22}\right)$$
$$+(1+\frac{3\mathsf{c}}{5})\grave{\mathbf{p}}_{40}+\frac{d_2}{4d_1}\left(\grave{\mathbf{p}}_{42}-\acute{\mathbf{p}}_{42}\right)+\frac{\mathsf{c}}{5}\grave{\mathbf{p}}_{50}+\frac{\mathsf{c}}{4d_1}\left(\grave{\mathbf{p}}_{52}-\acute{\mathbf{p}}_{52}\right);$$

$$\grave{\mathbf{p}}_{51} := \frac{2\mathsf{c}^2}{3d_1}\left(\mathsf{c}\grave{\mathbf{p}}_{00}+(3\mathsf{c}-5)\grave{\mathbf{p}}_{10}+5\grave{\mathbf{p}}_{11}\right)$$
$$+\frac{\mathsf{c}}{6d_1}\left(-16\mathsf{c}^2\grave{\mathbf{p}}_{20}+5(\mathsf{c}-4)(\grave{\mathbf{p}}_{21}-\acute{\mathbf{p}}_{21})+10(\grave{\mathbf{p}}_{22}-\acute{\mathbf{p}}_{22})\right)$$
$$-\mathsf{c}\grave{\mathbf{p}}_{40}+\frac{5\mathsf{c}}{4d_1}\left(\grave{\mathbf{p}}_{42}-\acute{\mathbf{p}}_{42}\right)+(1+\mathsf{c})\grave{\mathbf{p}}_{50}+\frac{4+3\mathsf{c}}{4d_1}\left(\grave{\mathbf{p}}_{52}-\acute{\mathbf{p}}_{52}\right).$$

For $i=3,4,5$, we get $\acute{\mathbf{p}}_{i1}$ from $\grave{\mathbf{p}}_{i1}$ by swapping $\grave{\mathbf{p}}$ with $\acute{\mathbf{p}}$.

B. Appendix: hybrid caps of degree bi-6

The bi-6 caps are internally G^1 according to

$$\partial_v\acute{\mathbf{f}}+\partial_v\grave{\mathbf{f}}-2\mathsf{c}(1-u)^2\partial_u\grave{\mathbf{f}}=0. \tag{6}$$

and they are C^1-connected to the last guided bi-6 surface ring. With the notations and indexing of Fig. 25a in the guide construction of Section 3.1, the unconstrained coefficient of the local solution to (6) are marked as bullets in Fig. 25a. The interactions between

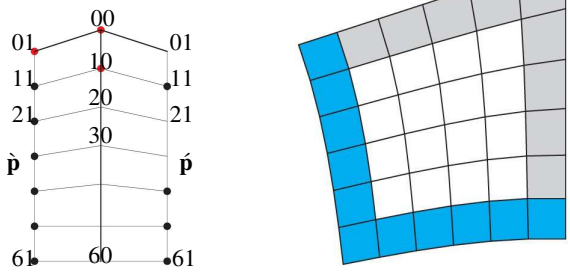

(a) indexing (b) reparameterization $\hat{\sigma}$

Figure 25: *(a) Local symmetric indexing: the unconstrained BB-coefficients are marked as red and black disks. (b) bi-6 reparameterization $\hat{\sigma}$ for sampling the guide.*

the n local G^1 systems of equations at the irregular point $\acute{\mathbf{p}}_{00} := \grave{\mathbf{p}}_{00}$ are resolved by selecting three BB-coefficients in one sector (red disks in Fig. 25a) to define the tangent plane at the irregular

point and define the corresponding BB-coefficients in other sectors recursively as

$$\grave{\mathbf{p}}_{10} := \grave{\mathbf{p}}_{10}\,, \quad \acute{\mathbf{p}}_{01} := -\grave{\mathbf{p}}_{01} + 2\mathsf{c}\grave{\mathbf{p}}_{10} + 2(1-\mathsf{c})\grave{\mathbf{p}}_{00}\,. \tag{7}$$

The explicit formulas for the dependent points of the local solution are

$$\begin{aligned}
\grave{\mathbf{p}}_{20} &:= \frac{3}{5\mathsf{c}}\left(\grave{\mathbf{p}}_{11}+\acute{\mathbf{p}}_{11}\right) + \left(\frac{6}{5}-\frac{6}{5\mathsf{c}}\right)\grave{\mathbf{p}}_{10} - \frac{1}{5}\grave{\mathbf{p}}_{00}\,;\\
\acute{\mathbf{p}}_{30} &:= \frac{1}{20}\left(\grave{\mathbf{p}}_{00}+\grave{\mathbf{p}}_{60}\right) - \frac{3}{10}\left(\grave{\mathbf{p}}_{10}+\grave{\mathbf{p}}_{50}\right) + \frac{3}{4}\left(\grave{\mathbf{p}}_{20}+\grave{\mathbf{p}}_{40}\right)\,;\\
\grave{\mathbf{p}}_{40} &:= \frac{1}{2}\left(\grave{\mathbf{p}}_{41}+\acute{\mathbf{p}}_{41}\right) + \frac{\mathsf{c}}{15}\left(\grave{\mathbf{p}}_{50}-\grave{\mathbf{p}}_{60}\right)\,;\\
\grave{\mathbf{p}}_{50} &:= \frac{1}{2}\left(\grave{\mathbf{p}}_{51}+\acute{\mathbf{p}}_{51}\right)\,, \quad \grave{\mathbf{p}}_{60} := \frac{1}{2}\left(\grave{\mathbf{p}}_{61}+\acute{\mathbf{p}}_{61}\right)\,;\\
\acute{\mathbf{p}}_{21} &:= -\grave{\mathbf{p}}_{21} - \frac{\mathsf{c}}{15}\grave{\mathbf{p}}_{00} + \frac{2\mathsf{c}}{5}\grave{\mathbf{p}}_{10} + (2-\mathsf{c})\grave{\mathbf{p}}_{20} + \mathsf{c}\grave{\mathbf{p}}_{40} - \frac{2\mathsf{c}}{5}\grave{\mathbf{p}}_{50} + \frac{\mathsf{c}}{15}\grave{\mathbf{p}}_{60}\,;\\
\acute{\mathbf{p}}_{31} &:= -\grave{\mathbf{p}}_{31} + \frac{1}{10}\grave{\mathbf{p}}_{00} - \frac{3}{5}\grave{\mathbf{p}}_{10} + \frac{3}{2}\grave{\mathbf{p}}_{20} + \frac{3-\mathsf{c}}{2}\grave{\mathbf{p}}_{40} + \frac{1-\mathsf{c}}{10}\left(\grave{\mathbf{p}}_{60}-6\grave{\mathbf{p}}_{50}\right)\,.
\end{aligned} \tag{8}$$

A bi-6 reparameterization $\hat{\sigma}$ for sampling the guide is rotationally and sector bisectrix symmetric and the outer BB-coefficients (blue underlay in Fig. 25b) C^1-extend the characteristic ring of Catmull-Clark-subdivision. This leaves 14 free parameters that are set to minimize the sum up to fifth derivatives, $\int_0^1\int_0^1 \sum_{i+j=5,i,j\geq 0} \frac{5!}{i!j!}(\partial_s^i\partial_t^j f(s,t))^2 dsdt$. Applying de Casteljau's algorithm at $u=\lambda^\ell = v$ to the sector of the guide and sampling $[\mathbf{g}^k\lambda^r\circ\hat{\sigma}]_{4\times 4}^6$ at all four corners of $\hat{\sigma}$ to form the bi-6 patch according to Fig. 4b implies that the resulting cap $\hat{\mathbf{g}}^k$ inherits the unique quadratic expansion of the guide. C^1-extending the last guided ring leaves $\grave{\mathbf{p}}_{21}$, $\grave{\mathbf{p}}_{31}$, $\acute{\mathbf{p}}_{21}$, $\acute{\mathbf{p}}_{31}$ (see Fig. 25a) to be the least squares best fit to the corresponding BB-coefficients of $\hat{\mathbf{g}}^k$ and $\hat{\mathbf{g}}^{k+1}$. As for $\mathbf{g}$ pretabulation simplifies practical computation.

Although the construction is formally only G^1, it is curvature continuous at the center and this partly accounts for its good shape.

C. Appendix: Eigenanalysis of the subdivision algorithm

Since the central point stays fix, the dominant eigenvalue is 1. Fig. 26 lists the indices of the other unconstrained control points $\mathcal{P}$ of the guide $\mathbf{g}$ (recall that red bullets labeled $1,\ldots,5$ are only unconstrained for sector $k=0$ and that for $n=3,6$ there is an additional degree of freedom at the location marked by a circled cross in Fig. 5b). With the abbreviations

$$n^* := \begin{cases} n+1, & \text{for } n\in\{3,6\},\\ n, & \text{else}\,,\end{cases}\,, \quad m := 6+n^*,$$
$$\bar{k} := 6+k; \quad \hat{k} := m+k; \quad dn^+ := dn+\hat{k},\ d=1,\ldots,16,$$

we label the $N := 17n+m-1$ elements of $\mathcal{P}$ as illustrated in Fig. 26.

After application of de Casteljau's algorithm at λ, the linearly-reparameterized bi-5 patches satisfy the *unchanged* constraints (1) and (2); this was intended and is verified by inspection. The mapping of $\mathcal{P}$ to its next-level counterpart yields systems of linear eigen-equations eq_i^s in unknowns x_j^s, $i,j=1,\ldots,N$, that form the eigenvectors corresponding to eigenvalues λ^s, $s=1,\ldots,10$. Solving the large and highly underconstrained systems with symbolic

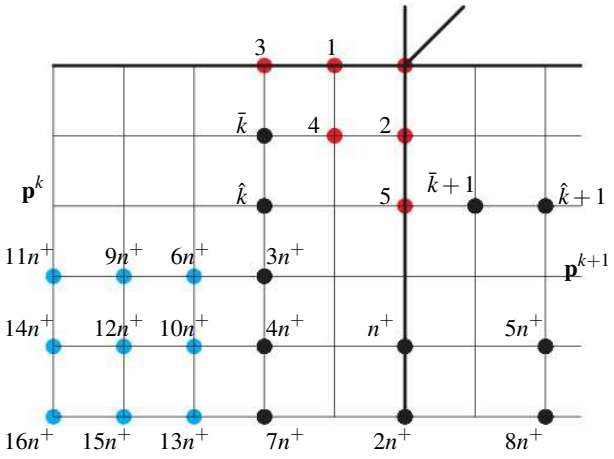

Figure 26: *Indices for the eigen-analysis.*

entries λ defies the capabilities of Maple, hence requires some careful guesses based on an observed pattern for concrete n and λ. The underconstrained systems are reduced by judiciously setting various x_i^s to zero and solving, for the specific $\lambda := \frac{1}{2}$, a subset of (system, variables)-pairs (eq_i^s, x_j^s). We abbreviate

$$a:b \quad := a, a+1, \ldots, b, \qquad \kappa(\alpha,\beta) := (m+\alpha n : m+\beta n-1).$$

For $s=1:10$, we list parameters set to zero, pairs of equations and variables, and the free parameters that will characterize the eigenvectors:

$s=$	$x^s_{1:j}=0$ $j=$	$(eq^s_{i:N}, x^s_{i:N})$ $i=$	x^s_k free $k=$
1		3	$1,2$
2	2	6	$3:5$
3	5	m	$6:m-1$
4	$m-1$	$2n+m$	$\kappa(0,2)$
5	$2n+m-1$	(I_5,J_5)	$\kappa(2,4)\cup\kappa(5,6)$
6	$4n+m-1$	$7n+m$	$\kappa(4,7)$
7	$7n+m-1$	(I_7,I_7)	$\kappa(7,8)\cup\kappa(9,11)$
8	$11n+m-1$	$14n+m$	$\kappa(11,14)$
9	$14n+m-1$	$16n+m$	$\kappa(14,16)$
10	$16n+m-1$		$\kappa(16,17)$

(9)

For $s=5$, system indices and variables differ: $I_5 := \kappa(5,17)$ and the variables are the union of labels $J_5 := \kappa(4,5)\cup\ \kappa(6,17)$. For $s=7$, $I_7 := \kappa(8,9)\cup\ \kappa(11,17)$. The system of equations eq_i^{10} is not listed since it is satisfied by setting $x^{10}_{1:j}=0$. The solutions of these systems are substituted into the initial systems with symbolic λ to verify that they solve the equations for any choice of λ. This yields explicit formulas for the eigenvectors in terms of the free parameters listed in the right column of (9). The eigenvectors, one per free parameter, span the eigenspace with the eigenvalues listed in Table (5).